RSC Advances

PAPER

View Article Online
View Journal | View Issue

Cite this: *RSC Adv.*, 2017, 7, 37310

Selective and confined growth of transition metal dichalcogenides on transferred graphene†

Fei Lu,[a] Arka Karmakar,[a] Simran Shahi[a] and Erik Einarsson *[ab]

Received 14th July 2017
Accepted 19th July 2017

DOI: 10.1039/c7ra07772f

rsc.li/rsc-advances

We demonstrate confinement of CVD grown MoS_2 to a patterned graphene area, forming a vertically stacked 2D heterostructure. The CVD-grown graphene had been transferred onto a Si wafer and patterned using photolithography. Raman mapping and spectral analysis reveal few-layer MoS_2 grew selectively on graphene regions, and not on the surrounding SiO_2 substrate surface. We also report CVD growth of WS_2 directly on transferred graphene. Unlike MoS_2, no few-layer regions were found; the WS_2 was found to be either monolayer or at least five layers (bulk). The WS_2 coverage was only partial, but selectivity to graphene is apparent. These findings have the potential to significantly advance fabrication of vertical 2D heterostructures and related devices, and suggest the selective growth on graphene may be applicable to TMDCs in general.

1 Introduction

As we continue to improve our understanding of two-dimensional (2D) materials, the focus of interest shifts increasingly toward 2D heterostructures. The atomically sharp interfaces in these so-called van der Waals solids give rise to unique properties that depend on the characteristics of their constituent layers.[1] Graphene and transition metal dichalcogenides (TMDCs) are the most thoroughly investigated 2D materials to date, and heterostructures based on these materials have yielded numerous potential applications including photodetectors,[2,3] photoresponsive memory devices,[4] field-effect transistors,[5,6] and quantum-well light-emitting diodes.[7] Many of these devices are based on vertically stacked 2D heterostructures, which are typically fabricated in one of three ways. One method is mechanical exfoliation, followed by manually picking and placing the exfoliated material at the desired location.[4,6,8] A second method is TMDC synthesis atop epitaxial graphene grown on a SiC substrate,[9–13] and a third is TMDC synthesis on graphene that has been transferred onto a silicon or quartz substrate.[2,3,5] One challenge common to all these methods is how to define the locations of these 2D heterostructures prior to growth. This hurdle must be overcome before fabrication techniques can be scaled beyond single elements.

Here we report CVD growth of molybdenum disulfide (MoS_2) directly atop, and laterally confined by, an underlying graphene pattern. We also report CVD synthesis of tungsten disulfide (WS_2) directly on graphene. While the WS_2 coverage was not complete, growth was selective to graphene and did not occur on the SiO_2 substrate surface. These results are an important step toward the ability to pre-define the growth location of 2D heterostructures by patterned graphene templates.

2 Experimental

To produce vertically stacked TMDC–graphene heterostructures, we first synthesized graphene at 1000 °C on copper foil using low-pressure chemical vapor deposition (CVD). We then transferred the graphene onto a silicon substrate with a 285 nm oxide layer (SiO_2/Si). This was done using an unpublished variation on a widely used wet process,[14,15] in which we use a copolymer layer in addition to a layer of poly(methyl methacrylate) (PMMA). We then used the graphene-on-SiO_2/Si as a substrate for TMDC growth (MoS_2 and WS_2). In the case of MoS_2 growth, we patterned the transferred graphene prior to CVD using standard photolithography techniques.

We grew MoS_2 by CVD in a tube furnace at 700 °C and atmospheric pressure. We prepared the molybdenum source by dispersing MoO_3 powder in ethanol, and then dropping the dispersion onto a 5 × 5 mm piece of silicon wafer.[16] After the ethanol evaporated, approximately 10 mg of MoO_3 remained. We then placed the patterned graphene-on-SiO_2/Si centered directly above the MoO_3 source at a distance of approximately 7 mm, with the patterned graphene side facing toward the MoO_3. The sulfur source was placed 30 cm upstream from the MoO_3 source (10 cm outside the furnace), and heated separately using a heating belt. Prior to CVD, we purged air from the system by

[a]Department of Electrical Engineering, University at Buffalo, Buffalo, NY, USA. E-mail: erikeina@buffalo.edu

[b]Department of Materials Design and Innovation, University at Buffalo, Buffalo, NY, USA

† Electronic supplementary information (ESI) available: Optical micrograph of MoS_2 on graphene, details regarding the curve fitting analysis of Raman spectra, and additional Raman spectra of MoS_2 on graphene, WS_2 on graphene, and graphene under various conditions are included. See DOI: 10.1039/c7ra07772f

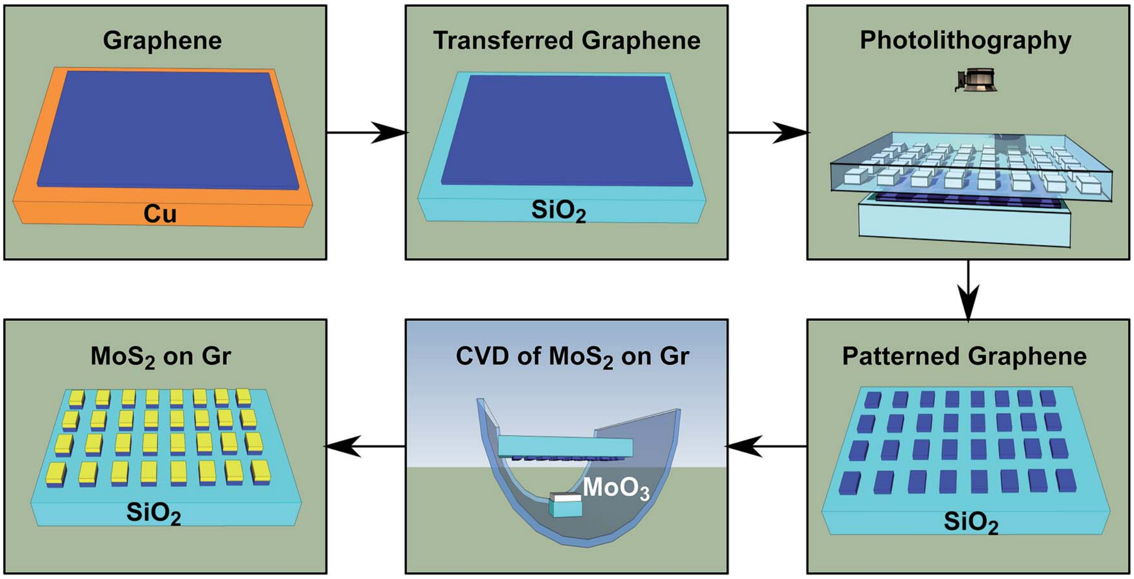

Fig. 1 Illustration of processing steps (clockwise from top left) resulting in localized CVD growth of MoS_2 on patterned graphene.

evacuating the quartz tube (26 mm ID) and refilling to atmospheric pressure using pure Ar gas. We continued to supply Ar at a flow rate of 150 sccm throughout the entire CVD process. We increased the furnace temperature by 20 °C per minute until reaching 700 °C, at which point the temperature was held constant for the duration of growth (10 min). The sulfur source was kept at 200 °C throughout. An overview of the process is illustrated in Fig. 1.

The process for WS_2 growth was similar to that for MoS_2, except that growth occurred at 900 °C instead of 700 °C. One minor difference is a longer growth time for WS_2 (15 min instead of 10 min). The tungsten source was also prepared as is common for CVD growth of WS_2, but this is different to the Mo source preparation. We simply placed 100 mg of WO_3 powder in a quartz boat and positioned it below the target substrate as described above. The placement of the sulfur source was identical in both cases, but we note that these growth procedures have not been fully optimized.

After TMDC growth, we characterized the results using optical microscopy and Raman spectroscopy. We used a Renishaw inVia Reflex micro-Raman spectrometer to collect Raman spectra and perform mapping. Excitation laser wavelengths were 514 nm for MoS_2 and 488 nm for WS_2 in order to avoid strong resonances at 514 nm.[17]

3 Results and discussion

3.1 MoS_2 growth localized to patterned graphene

The top row of Fig. 2(a)–(c) shows an optical micrograph of as-grown MoS_2–graphene heterostructures and two superimposed Raman intensity maps. The Raman map in Fig. 2(b) shows the graphene 2D peak intensity, confirming graphene in the patterned rectangles. The other Raman map in Fig. 2(c) shows the integrated intensity of the two characteristic MoS_2 peaks found between 370 cm^{-1} and 420 cm^{-1}. Both Raman maps correspond to the same area, confirming MoS_2 growth was directly atop, and confined by, patterned graphene.

In the upper panel of Fig. 2d, we show Raman spectra before and after MoS_2 growth on graphene. These are labeled (i) and (ii), respectively. In addition to the graphene G and 2D peaks,[18] additional peaks appear after MoS_2 growth. Based on the decomposition and fitting shown in Fig. 2e, we attribute the small, emergent Raman peaks located at 1259 cm^{-1} and 1456 cm^{-1} to C–H stretching and bending modes.[19] Although these peaks only appear when sulfur is supplied, the positions and relative intensities more closely match peaks associated with C–H than C–S bonds.[20] The origin of hydrogen, however, is not clear. We attribute the larger peaks at 1376 cm^{-1}, 1559 cm^{-1}, and 2887 cm^{-1} to the D, G, and 2D peaks of amorphous carbon ($D_{a\text{-}C}$, $G_{a\text{-}C}$, $2D_{a\text{-}C}$).[21]

In the lower panel of Fig. 2d we show Raman spectra from graphene-on-SiO_2/Si annealed at the MoS_2 growth temperature (700 °C). When annealed under pure Ar (Fig. 2d(iii)), no peaks associated with a-C appear. When annealed in the presence of sulfur but in the absence of MoO_3 (Fig. 2d(iv)), a-C peaks are clearly visible, and the spectrum is very similar to that of MoS_2 grown on graphene (Fig. 2d(ii)). These results indicate that a-C formation is not simply due to elevated temperature, but the presence of sulfur at elevated temperature.[20] In spite of this, the amount of a-C can be reduced by annealing in a sulfur environment at even higher temperature. This is shown in Fig. 2d(v), which corresponds to MoS_2 on graphene annealed at 900 °C for 20 min in the presence of sulfur. We note that the a-C Raman modes have considerably lower relative intensity, whereas the other peaks remain largely unchanged.

All spectra in Fig. 2d exhibit an upshift of the graphene G and 2D peaks, as well as broadening of the 2D peak relative to the as-transferred graphene. These changes suggest hole doping of the graphene occurs during thermal treatment[22,23] and subsequent exposure to the atmosphere.[24]

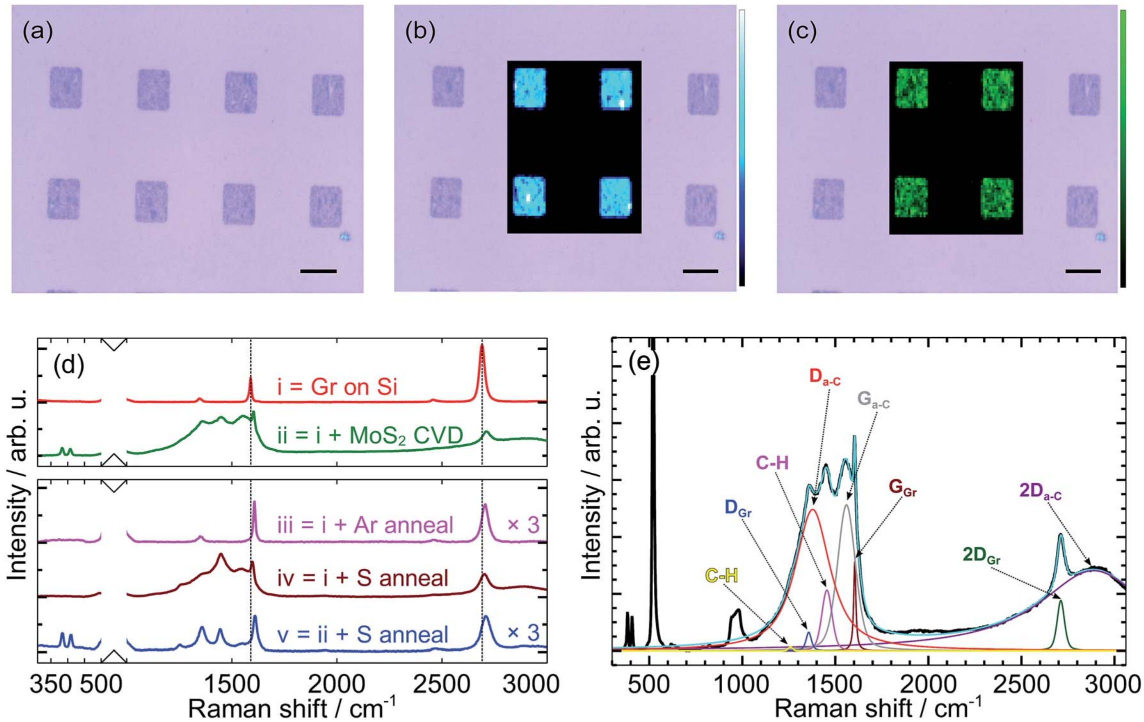

Fig. 2 (a) Optical micrograph of patterned graphene on SiO_2/Si. Scale bar corresponds to 20 μm. (b and c) Superimposed Raman maps showing MoS_2 growth corresponds exactly to graphene pattern regions. (b) Intensity of graphene 2D peak at 2711 cm^{-1} and (c) integrated intensity of MoS_2 E^1_{2g} and A_{1g} peaks (from 370 to 420 cm^{-1}). (d) Raman spectra of (i) graphene, (ii) MoS_2 on graphene, and (iii–v) annealed versions of both. All spectra are normalized to the first-order silicon peak (hidden), and $\lambda_{ex} = 514$ nm. (e) Decomposition of Raman spectrum after CVD of MoS_2 on graphene ((ii) in (d)).

Based on the positions of the MoS_2 E^1_{2g} and A_{1g} Raman modes,[25,26] we find the MoS_2 thickness ranges from two layers to five or more layers (bulk), with the majority being three or four layers of MoS_2. We found the layer number to be very sensitive to the local MoO_3 concentration. Near the center of the substrate, where the MoO_3 concentration is highest (*i.e.*, directly above the MoO_3 source), we find MoS_2 can nucleate and grow directly on the silicon wafer, but is predominantly bulk. Closer to the substrate edge, where the MoO_3 concentration is lower, few-layer MoS_2 selectively grows only on graphene. Our hypothesis for the selective growth on graphene is as follows. Since sulfur is introduced to the system from the beginning of the CVD process, it can satisfy dangling bonds present in graphene. When the growth temperature is reached and Mo is present, the attached sulfur atoms act as nucleation sites, leading to selective growth of MoS_2 on graphene. This mechanism should also apply to other TMDCs under appropriate conditions, and the following results for WS_2 suggest that to be the case.

3.2 WS_2 grown directly on graphene

Fig. 3a shows an optical image of WS_2 grown on graphene by CVD. We note that patterned graphene was not used here. Instead, we reduced the CVD time in order to avoid forming continuous graphene, and then grew WS_2 atop that. Raman intensity maps of the graphene 2D and WS_2 E^1_{2g} peaks are shown in Fig. 3b and c. The mapped area corresponds to the dotted outline in Fig. 3a. Comparing the Raman maps with the optical micrograph, we see that the majority of the surface is covered by graphene, but only some of the graphene is covered by WS_2. Darker regions in (a) are WS_2 on top of graphene, whereas bright spots correspond to bulk WS_2 (five or more layers). A few graphene voids are visible as slightly lighter patches. WS_2 appears to grow right up to the edge of several of these voids, but does not extend out onto the SiO_2 surface. This indicates that WS_2 grows selectively on graphene, as was the case for MoS_2.

In Fig. 3d we plot various Raman spectra for comparison. The top two spectra are from the Raman maps shown, whereas the bottom three spectra are from different processes but shown for comparison and clarification. Our analysis reveals several similarities with MoS_2 grown on graphene. For example, we find C–H peaks in the Raman spectra for both cases. Despite the presence of sulfur during WS_2 growth at 900 °C, no obvious a-C Raman peaks are found. This is consistent with our finding that annealing MoS_2 at this temperature in a sulfur environment reduced the amount of a-C. Lowering the WS_2 growth temperature from 900 °C to 850 °C increased coverage of WS_2 on graphene, but the quality of graphene suffered (*i.e.*, strong C–H and a-C peaks appeared).

Based on the E^1_{2g} and A_{1g} peak separation,[17] one significant difference between WS_2 on graphene and MoS_2 on graphene is that we find no few-layer regions of WS_2. The WS_2 grown on graphene is either monolayer (ML) or bulk (5+ layers).

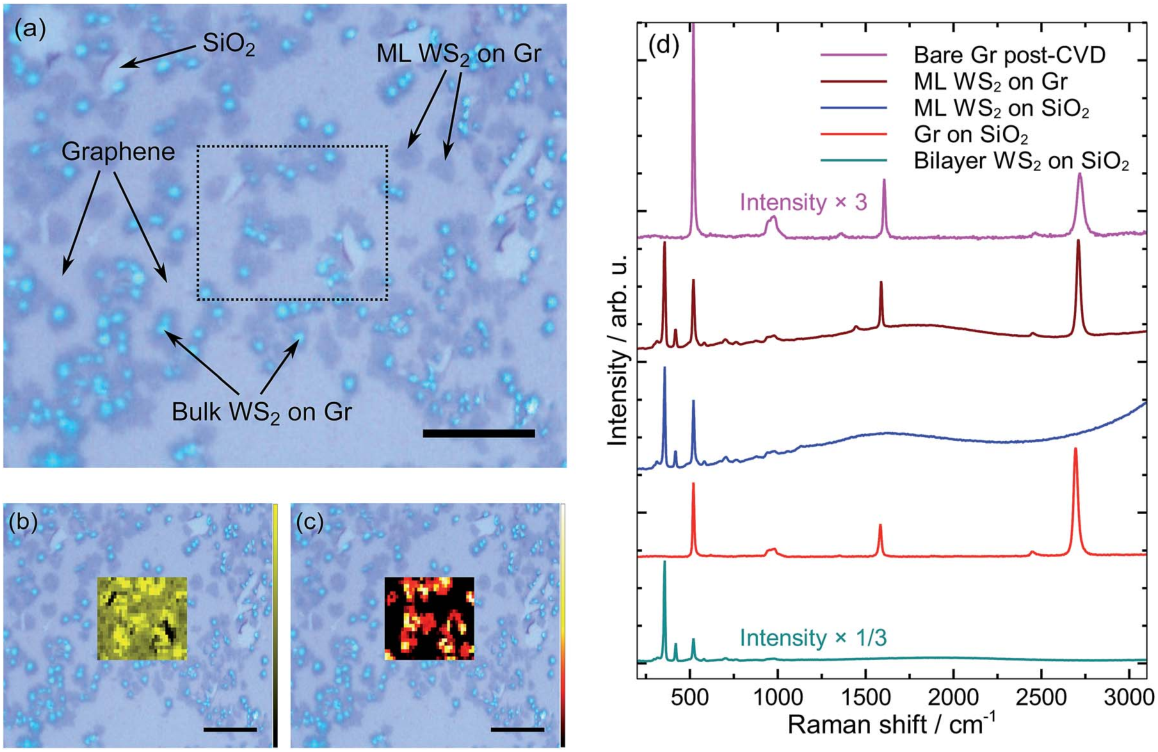

Fig. 3 (a) Optical micrograph of WS_2 grown on graphene. Dotted line denotes mapped area shown in (b and c). All scale bars are 20 μm, and λ_{ex} = 488 nm. (b) Intensity map of graphene 2D peak at 2727 cm^{-1}. (c) Intensity map of E^1_{2g} peak of monolayer WS_2 at 354.9 cm^{-1}. (d) Raman spectra of graphene and WS_2 with different interfacial conditions. The topmost two spectra are from the map at left, whereas the lower three spectra are from different processes and shown for comparison. All spectra are normalized to the first-order silicon peak.

Importantly, we noticed small shifts in the E^1_{2g} and A_{1g} peak positions for ML WS_2 on graphene compared to ML WS_2 on SiO_2/Si. The E^1_{2g} peak position shifts down slightly from 355.6 cm^{-1} to 355.1 cm^{-1}, whereas the A_{1g} peak shifts up slightly from 417.2 cm^{-1} to 417.6 cm^{-1}. This is only slightly larger than the uncertainty of 0.3 cm^{-1}, but the shift is consistent for more than 10 independent measurements. We find the E^1_{2g} and A_{1g} peak separation for monolayer WS_2 on graphene to be 62.5 cm^{-1}. This is slightly larger than the 61.6 cm^{-1} for WS_2 on SiO_2, yet still less than the 63.4 cm^{-1} that corresponds to bilayer WS_2 on SiO_2.[17]

By comparing the WS_2 E^1_{2g} and A_{1g} peak intensities to the Si substrate peak at 520 cm^{-1}, we can confirm the darker regions seen in Fig. 3a are indeed monolayer rather than bilayer WS_2 on graphene. The presence of a fluorescence tail (onset visible near 3000 cm^{-1}) is further evidence that the spectrum labeled "ML WS_2 on SiO_2" is indeed monolayer. The absence of this tail for monolayer WS_2 on graphene is due to ultrafast charge transfer to graphene,[27] indicating a clean and sharp interface in the heterostructure. Moreover, the strong Raman signal suggests graphene quality remains high despite the high-temperature growth environment.

4 Conclusion

In conclusion, we report CVD growth of few-layer MoS_2 directly atop patterned graphene in which the MoS_2 is confined to the graphene region. The MoS_2 covered the entire graphene pattern, demonstrating the ability to define the shape and location of vertically stacked 2D heterostructures prior to CVD. We also report WS_2 selectively grown on transferred graphene. Unlike MoS_2, coverage of WS_2 was incomplete, and was found to be either bulk or monolayer. Obtaining complete coverage of WS_2 should be a matter of finding appropriate growth conditions and is left for future study. For both MoS_2 and WS_2, we hypothesize that sulfur atoms that satisfy dangling bonds on the graphene act as nucleation sites, confining the growth location. Similar findings using two different TMDCs, despite considerably different growth conditions, suggests this graphene-templated selective growth may apply to TMDCs in general. We expect these results will facilitate batch fabrication of 2D heterostructure systems and devices.

Acknowledgements

This work was supported by Award FA9550-16-1-0188 from the Air Force Office of Scientific Research, and by the Innovative Micro-Programs Accelerating Collaboration in Themes (IMPACT) program funded by the Office of Vice President of Research and Economic Development at the University at Buffalo.

References

1 A. C. Ferrari, F. Bonaccorso, V. Fal'ko, K. S. Novoselov, S. Roche, P. Bøggild, S. Borini, F. H. L. Koppens,

V. Palermo, N. Pugno, J. A. Garrido, R. Sordan, A. Bianco, L. Ballerini, M. Prato, E. Lidorikis, J. Kivioja, C. Marinelli, T. Ryhänen, A. Morpurgo, J. N. Coleman, V. Nicolosi, L. Colombo, A. Fert, M. Garcia-Hernandez, A. Bachtold, G. F. Schneider, F. Guinea, C. Dekker, M. Barbone, Z. Sun, C. Galiotis, A. N. Grigorenko, G. Konstantatos, A. Kis, M. Katsnelson, L. Vandersypen, A. Loiseau, V. Morandi, D. Neumaier, E. Treossi, V. Pellegrini, M. Polini, A. Tredicucci, G. M. Williams, B. H. Hong, J.-H. Ahn, J. M. Kim, H. Zirath, B. J. van Wees, H. van der Zant, L. Occhipinti, A. Di Matteo, I. A. Kinloch, T. Seyller, E. Quesnel, X. Feng, K. Teo, N. Rupesinghe, P. Hakonen, S. R. T. Neil, Q. Tannock, T. Löfwander and J. Kinaret, *Nanoscale*, 2015, **7**, 4598–4810.

2 C. Chen, Z. Feng, Y. Feng, Y. Yue, C. Qin, D. Zhang and W. Feng, *ACS Appl. Mater. Interfaces*, 2016, **8**, 19004–19011.

3 W. Zhang, C.-P. Chuu, J.-K. Huang, C.-H. Chen, M.-L. Tsai, Y.-H. Chang, C.-T. Liang, Y.-Z. Chen, Y.-L. Chueh, J.-H. He, M.-Y. Chou and L.-J. Li, *Sci. Rep.*, 2014, **4**, 3826.

4 K. Roy, M. Padmanabhan, S. Goswami, T. P. Sai, G. Ramalingam, S. Raghavan and A. Ghosh, *Nat. Nanotechnol.*, 2013, **8**, 826–830.

5 M. Zhao, Y. Ye, Y. Han, Y. Xia, H. Zhu, S. Wang, Y. Wang, D. A. Muller and X. Zhang, *Nat. Nanotechnol.*, 2016, **11**, 954–959.

6 T. Georgiou, R. Jalil, B. D. Belle, L. Britnell, R. V. Gorbachev, S. V. Morozov, Y.-J. Kim, A. Gholinia, S. J. Haigh, O. Makarovsky, L. Eaves, L. A. Ponomarenko, A. K. Geim, K. S. Novoselov and A. Mishchenko, *Nat. Nanotechnol.*, 2013, **8**, 100–103.

7 F. Withers, O. Del Pozo-Zamudio, A. Mishchenko, A. P. Rooney, A. Gholinia, K. Watanabe, T. Taniguchi, S. J. Haigh, A. K. Geim, A. I. Tartakovskii and K. S. Novoselov, *Nat. Mater.*, 2015, **14**, 301–306.

8 L. Britnell, R. M. Ribeiro, A. Eckmann, R. Jalil, B. D. Belle, A. Mishchenko, Y.-J. Kim, R. V. Gorbachev, T. Georgiou, S. V. Morozov, A. N. Grigorenko, A. K. Geim, C. Casiraghi, A. H. Castro Neto and K. S. Novoselov, *Science*, 2013, **340**, 1311–1314.

9 Y. Shi, W. Zhou, A.-Y. Lu, W. Fang, Y.-H. Lee, A. L. Hsu, S. M. Kim, K. K. Kim, H. Y. Yang, L.-J. Li, J.-C. Idrobo and J. Kong, *Nano Lett.*, 2012, **12**, 2784–2791.

10 C. E. Giusca, I. Rungger, V. Panchal, C. Melios, Z. Lin, Y.-C. Lin, E. Kahn, A. L. Elías, J. A. Robinson, M. Terrones and O. Kazakova, *ACS Nano*, 2016, **10**, 7840–7846.

11 A. Rossi, H. Büch, C. D. Rienzo, V. Miseikis, D. Convertino, A. Al-Temimy, V. Voliani, M. Gemmi, V. Piazza and C. Coletti, *2D Materials*, 2016, **3**, 031013.

12 Y.-C. Lin, C.-Y. S. Chang, R. K. Ghosh, J. Li, H. Zhu, R. Addou, B. Diaconescu, T. Ohta, X. Peng, N. Lu, M. J. Kim, J. T. Robinson, R. M. Wallace, T. S. Mayer, S. Datta, L.-J. Li and J. A. Robinson, *Nano Lett.*, 2014, **14**, 6936–6941.

13 D. Pierucci, H. Henck, C. H. Naylor, H. Sediri, E. Lhuillier, A. Balan, J. E. Rault, Y. J. Dappe, F. Bertran, P. L. Fèvre, A. T. C. Johnson and A. Ouerghi, *Sci. Rep.*, 2016, **6**, 26656.

14 X. Li, Y. Zhu, W. Cai, M. Borysiak, B. Han, D. Chen, R. D. Piner, L. Colombo and R. S. Ruoff, *Nano Lett.*, 2009, **9**, 4359–4363.

15 G. B. Barin, Y. Song, I. F. Gimenez, A. G. Souza Filho, L. S. Barreto and J. Kong, *Carbon*, 2015, **84**, 82–90.

16 Z. Lin, Y. Zhao, C. Zhou, R. Zhong, X. Wang, Y. H. Tsang and Y. Chai, *Sci. Rep.*, 2015, **5**, 18596.

17 A. Berkdemir, H. R. Gutiérrez, A. R. Botello-Méndez, N. Perea-López, A. L. Elías, C.-I. Chia, B. Wang, V. H. Crespi, F. López-Urías, J.-C. Charlier, H. Terrones and M. Terrones, *Sci. Rep.*, 2013, **3**, 1–8.

18 A. C. Ferrari, J. C. Meyer, V. Scardaci, C. Casiraghi, M. Lazzeri, F. Mauri, S. Piscanec, D. Jiang, K. S. Novoselov, S. Roth and A. K. Geim, *Phys. Rev. Lett.*, 2006, **97**, 187401.

19 H. Wu, J. V. Volponi, A. E. Oliver, A. N. Parikh, B. A. Simmons and S. Singh, *Proc. Natl. Acad. Sci. U. S. A.*, 2011, **108**, 3809–3814.

20 L. Zhang, L. Ji, P.-A. Glans, Y. Zhang, J. Zhu and J. Guo, *Phys. Chem. Chem. Phys.*, 2012, **14**, 13670–13675.

21 J. Hong, M. K. Park, E. J. Lee, D. Lee, D. S. Hwang and S. Ryu, *Sci. Rep.*, 2013, **3**, 2700.

22 S. Ryu, L. Liu, S. Berciaud, Y.-J. Yu, H. Liu, P. Kim, G. W. Flynn and L. E. Brus, *Nano Lett.*, 2010, **10**, 4944–4951.

23 J. E. Lee, G. Ahn, J. Shim, Y. S. Lee and S. Ryu, *Nat. Commun.*, 2012, **3**, 1024.

24 L. Liu, S. Ryu, M. R. Tomasik, E. Stolyarova, N. Jung, M. S. Hybertsen, M. L. Steigerwald, L. E. Brus and G. W. Flynn, *Nano Lett.*, 2008, **8**, 1965–1970.

25 C. Lee, H. Yan, L. E. Brus, T. F. Heinz, J. Hone and S. Ryu, *ACS Nano*, 2010, **4**, 2695–2700.

26 H. Li, Q. Zhang, C. C. R. Yap, B. K. Tay, T. H. T. Edwin, A. Olivier and D. Baillargeat, *Adv. Funct. Mater.*, 2012, **22**, 1385–1390.

27 J. He, N. Kumar, M. Z. Bellus, H.-Y. Chiu, D. He, Y. Wang and H. Zhao, *Nat. Commun.*, 2014, **5**, 5622.